Journal of Energy and Power Engineering 10 (2016) 23-31
doi: 10.17265/1934-8975/2016.01.003

The Mechanism of Flow Field around a Rotating Cylinder with Fins for High Performance Magnus Wind Turbine

Nobuhiro Murakami[1], Hiroaki Hasegawa[2], Toshihiro Haniu[1] and Masahide Nakamura[1]

1. Dept. of Mechanical Engineering Tegatagakuen-machi 1-1, Graduate School of Engineering & Resource Science, Akita Univ., Akita 010-8502, Japan

2. Dept. of Mechanical and Intelligent Engineering Yoto, Graduate School of Engineering, Utsunomiya Univ., Utsunomiya-shi 7-1-2, Japan

Received: November 23, 2015 / Accepted: December 02, 2015 / Published: January 31, 2016.

Abstract: Spiral Magnus is a unique wind turbine system that rotates with cylinders which have spiral-shaped fins coiled around them (instead of using the more common propeller-type blades). In the present study, three models (cylinder with no fins, cylinder with straight fins and cylinder with spiral fins) were installed, and fluid force measurements were performed by a strain gauge force balance. A PIV (particle image velocimetry) system was used to better understand the flow fields around the cylinder. Considering the results of the experiment, it was confirmed that, the aerodynamic performance of the rotating cylinder can be improved by the fin. However, the straight fin makes the flow close to the cylinder surface ineffective. The rotary cylinder with the spiral fins was able to generate the greatest lift among three models, because the spiral fin effectively influences the vicinity of the cylinder surface.

Key words: Wind turbine, Magnus effect, wind tunnel test, spiral Magnus.

Nomenclature

C_L	Time-averaged lift coefficient
d	Cylinder diameter (m)
Re	Reynolds number
U	Free stream direction velocity (m/s)
U_0	Free stream velocity (m/s)
V_S	Cylindrical surface speed (m/s)
α	Rotational angle (°)
θ	Circumferential speed ratio
ν	Kinematic coefficient of viscosity (m^2/s)
Ω	Vorticity
ω	Angular velocity (rad/s)

1. Introduction

The development of wind power generation from large wind turbines has shown excellent profitability, therefore, this form of renewable energy construction is accelerating as mainstream around the world. However, these businesses must be built in locations away from residential area, from the point of view of the landscape and noise. Wind power generation also requires that, wind conditions be good and the site be near an electric power-consuming region. However, locations fulfilling such conditions are few. Therefore, a small wind turbine with superior quietness and high performance is demanded. This would allow extensive construction near residential areas. In addition, development and maintenance of the transmission line would also be cheaper.

A Magnus wind turbine uses a rotating cylinder as a substitution for the blade of a common wind turbine. When the cylinders rotate, lift is generated. This lift is sufficient to generate electricity by rotating the wind turbine to which the cylinders are attached. The wing of the wind turbine is in a column shape, and, in the Magnus wind turbine, the power performance rises so that the lift becomes bigger. After the invention of a

Corresponding author: Nobuhiro Murakami, doctor, research fields: engineering, aero dynamics and wind turbine.

large performance enhancement in 2004 by adding a spiral fin to the column, and after applying for a patent [1], commercialization is being advanced. The spiral Magnus wind turbine obtains significant lift from even low wind speeds (Fig. 1). It can be seen to have under stable output characteristics even under rapid wind velocity fluctuations. Therefore, the relatively high resulting amount of cumulative generated power from the small wind turbine "swept area below 200 square meters" is shown as superior power generation performance [2]. According to the actual measurement results, approximately 8% of the generated power is used to rotate the rotary cylinder. However, in order to accelerate commercialization, it is desirable to improve performance even more. Therefore, the elucidation of the flow mechanisms that occur between the mainstream and the spiral cylindrical wing is important.

Previous studies had the purpose of optimizing the spiral fin shape. These investigations, which primarily focused on the comparative analysis of various spiral shapes, were carried out in wind tunnel experiments, computer simulation studies, and actual on-site testing of several kinds of models [3, 4]. However, there has not been enough elucidation of the flow field and the mechanism of rotation around the finned cylinder. There are still many possibilities for performance improvement. This study intended to clarify the lift-generating mechanism in the flow field around a rotating cylinder with fin. By considering the mechanism in the light of the state of the fluid force and the generated flow field, the mechanism of lift generation was revealed.

2. Experimental Apparatus and Methods

2.1 Experimental Setup

A schematic of the measurement section of the present study is shown in Fig. 2. The wind tunnel was an open type, with an outlet of 300 mm × 300 mm. The rotation cylinder models were placed in the test section. The DC motor (S12280-240, Special Electrical

Fig. 1 The spiral Magnus wind turbine at Akita marina (March 2011 start-up).

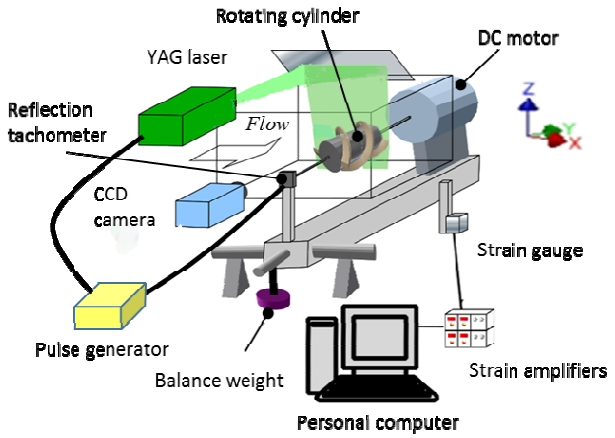

Fig. 2 Schematic of experimental setup.

Co.) rotated the cylinder. The rotation unit, including the model and the motor, was structured to move as a balance about the fulcrum, therefore, a weight was placed on the front side of the fulcrum. As the rotation unit moved about the fulcrum, owing to the lift generated as the flow passed over the rotating cylinder, the strain gauge indirectly measured the lift. In the visualization and PIV (particle image velocimetry) process, the transmitted laser sheet was deflected by the mirror. Relative to the longitudinal direction of the model was established as extending from the upper vertical. The PIV system mainly consists of CCD (charge-coupled device) cameras (Mega plus ES1.0, 1,008 × 1,024 pixels, Kodak Co. Ltd.), a Nd-YAG laser (Solo 120XT, New Wave Research, Inc.), a pulse generator (Quantum Composers, Inc., 9314), a rotary

encoder (Ono Sokki LG-919) and a smoke generator (Kano Max, 8304). Tracer using an oil mist, the particle size is about 1 μm. Rotational speed of the cylinder with blades was measured using a reflection tachometer. The timing of the laser irradiation is synchronized by a pulse generator.

2.2 Experimental Methods

The origin of the coordinate system was the center of gravity of the experimental model. The main flow direction was X, the measurement unit span direction was Y, and the height direction was Z. The free stream Reynolds number (*Re*) of flow around a cylinder, with a typical dimension for the column diameter $d = 0.07$ m, and the representative speed is the mainstream velocity $U_0 = 4$ m/s, was from $Re = 1.9 \times 104$. The mainstream and the ratio of the rotary speed of the column θ are the important parameters for showing the state. The flow field around the cylinder, the outer flow $1/2d\omega$, and the mainstream U_0 due to the rotation of the cylinder. Eq. (1) shows the velocity ratio as a circumferential speed ratio θ.

$$\theta = \frac{d\omega}{2U_0} \tag{1}$$

Lift measurements were conducted using three types of experimental models for $\theta = 0$-1.1. The strain gauge, using a two-component force meter that was proven in previous experiments [5, 6], using that single component force. The measurement data, 5,000 data points acquired at a sampling speed of 500 μs, was carried out six times, and is determined as an average value. The error in this measurement is about 1.9%. The flow velocity distribution of the flow field around a rotating cylinder was determined by PIV. In addition, the peripheral speed ratio at this time is $\theta = 1$. The irradiation laser was carried out in two consecutive passes, the irradiation interval, and the 500 μs. The width of the laser sheet was 5 mm. We analyzed the images in the PIV software (FtrPIV, FLOWTECH RESEARCH Corp.). However, the laser irradiated from the upper side of the model, and hence, it was not possible to photograph the entire flow field. Therefore, to complete the model, the data from the upper half of the surface were reversed for the model surface of the lower half, and the upper and lower data were then synthesized by the X-axis reference.

2.3 Experimental Models

Fig. 3 shows in three experimental models. Fig.3a is the reference made no cylinder of the fin. Fig. 3b is a cylinder with straight fin cylinder (dual). Fig. 3c is a cylinder with a spiral fin (dual). Straight fins with 10 mm width and 18 mm height is placed in parallel to the Y axis, and the other one was placed similarly in a

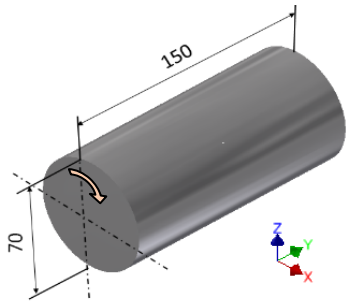

(a) No fin

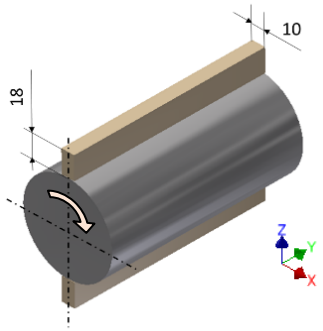

(b) Straight fins (dual)

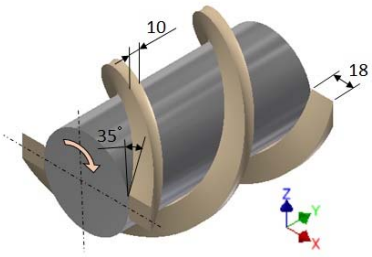

(c) Spiral fins (dual)

Fig. 3 Three types of test models (dimensions in mm).

position which is shifted 180°. Spiral fins, was a left-handed in a 35° and its width is 10 mm, the fin height of 18 mm as a starting point to any point of the cylinder end face. And the other one was placed similarly in a position which is shifted 180°.

3. Experimental Results and Consideration

3.1 Lift Measurement

Fig. 4 gives the lift measurement results for the three models. In addition, it shows the $C_L = 2\pi\theta$ derived from the potential theory, with the lift of an ideal fluid as a reference. In the $\theta = 1$ neighborhood, the lift for the spiral fins and straight fins became larger than that without fins. In particular, the rotating cylindrical blade that was added to the spiral fins had a circumferential speed ratio $\theta = 1$ showed high lift conforming to $C_L = 2\pi\theta$ of an ideal fluid. In addition, the straight fins and spiral fins also increased lift with increasing θ. When $\theta > 1$, lift began to converge to a constant value. However, the model without fins continued to increase. When the value of θ was less than 1, the fins acted to increase the lift. Changes in the work of the fin begin to occur in the vicinity of $\theta = 1$. The reason for this is described in the "PIV measurement around a cylinder" section of this paper. When the windmill is running, there is actually always a value of θ for receiving a pulsation of wind changes. In Fig. 4, the lift is high in the vicinity of the circumferential speed ratio θ = 0.9-1.1 for the spiral fin. It was shown that, there was little change in the lift values for θ. This means the wind turbine is insensitive to the pulsation of the wind. The range of the optimum power condition is a feature leading to an increase in the wide power generation. However, when the actual wind turbine is turning, the tip and the root of the cylinder blades are different distances from the center of the wind turbine. Therefore, in an actual wind turbine, it is necessary to consider that, if a triangular vector is generated between the main flow and the flow due to the turning of the wind turbine, it is not the same near the root as it is at the tip. In the rotating cylinder, the velocity triangle of flow

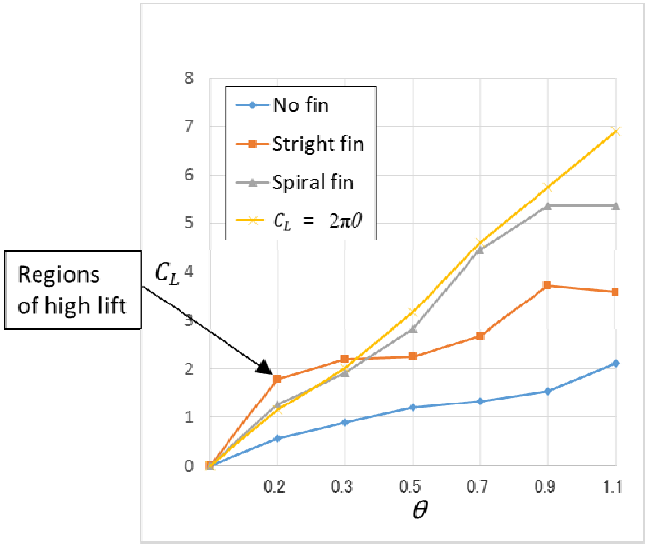

Fig. 4 Coefficient of lift.

flowing in each radial position is different. Therefore, it is a complex flow. Hence, when designing an actual wind turbine, it is necessary to consider that, the influence of the circumferential speed ratio is different in the radial direction of the rotating cylinder.

3.2 PIV Measurement of around a Cylinder

For the lift measurement at the time of changes in the circumferential speed ratio, a different trend was obtained for each model. To test the cause of this, two flow field straight fins and the spiral fin were examined by PIV measurements. The measurement results indicate the direction and speed of the flow vector, as well as the distribution of the main flow direction velocity U as a gradient. The vertical and horizontal axes in the figure, each with a diameter of the cylinder, are dimensionless by mainstream wind speed U_0. Additionally, the speed of the data is averaged for the result of the PIV processing of 40 sets of particle images. Considering the potential flow around the rotating cylinder in Fig. 5, the cylindrical surface speed V_S generated by the rotation of the cylinder as the direction and magnitude is the symmetry at the top and bottom of the cylinder. Cylindrical surface speed V_S, induced by rotation, is generated in the A section. On the other hand, the cylindrical surface speed of the B portion, the reverse side, is $-V_S$. On the reverse flow

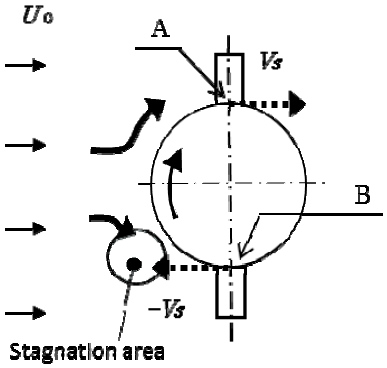

Fig. 5 Situation of flow past around circular cylinder (α = 0°).

side of the cylinder, a stagnation region is formed by interference between the main flow and the flow due to this rotation.

Fig. 6 shows a straight finned rotating cylinder in the mainstream, a flow field image taken at the moment of each rotation angle α. The flow is periodically deformed by the rotational angle. Rotating cylinders with straight fins affect to the flow velocity distribution in a far area from the cylinder. In the measurement of the lift of Fig. 4, in the case of θ = 1, finned cylinders show a high lift. In the part A of Fig. 5, the flow of the cylindrical surface speed V_S and mainstream speed U_0 is the same. In the forward flow side, these flows are similar, which is a unique state. Accordingly, since the fins through the forward flow side of the main flow move synchronously at the same speed, the influence that the fins exert on the periphery of the flow is the lowest state. Furthermore, when we focus on the formation of the stagnation region, we see that it forms a large area, as shown in Fig. 6d. Thus, the impact of the stagnation region, in which U_0 and -V_S is in the

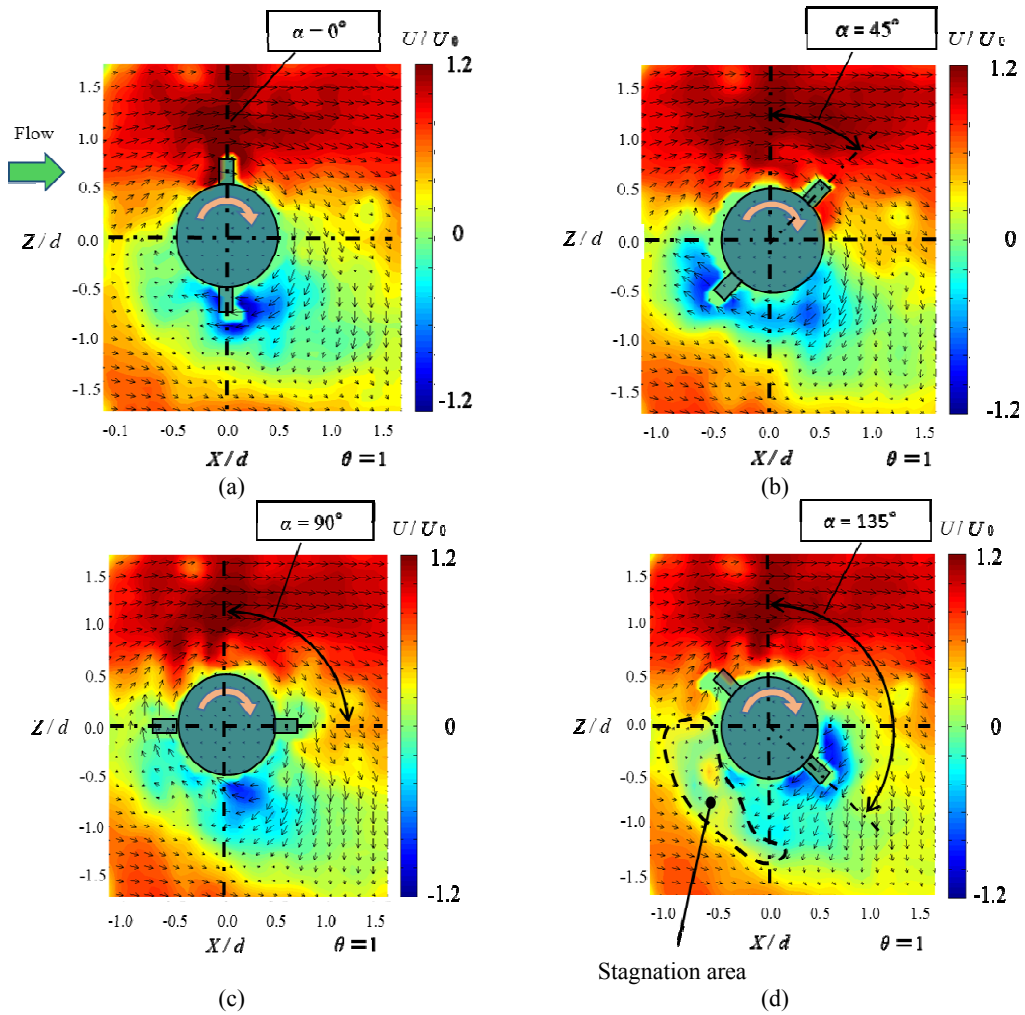

Fig. 6 Flow past around circular cylinder with straight fins: 4 angle conditions (θ = 1).

reverse direction flow, shows that, side collisions become a major factor of lift generation. This is one of the reasons that high lift is generated from the time of relatively low Reynolds number.

Figs. 7 and 8 exhibit the measurement results, indicating the direction and speed of the flow vector and showing the distribution of vorticity as the gradient. For Fig. 4, we discussed the results of the measurement of the lift for the straight fin. A rapid increase in lift is seen when the value of θ is in the vicinity of 0.2-0.4. This is an area that exhibits lift values greater than the lift line of an ideal fluid. Fig. 4 shows a high lift when the circumferential speed ratio $\theta = 0.2$. Therefore, Fig. 7 shows the vorticity for the case of $\theta = 0.2$, for rotation angles at: (a) $\alpha = 0°$, (b) $\alpha = 45°$, (c) $\alpha = 90°$, (d) $\alpha = 135°$.

In the forward flow seen in Fig. 7d, when $\alpha = 135°$, a strong vorticity near the backward cylinder fin (blue—clockwise vorticity) is generated. Then, in Fig. 7b, in which $\alpha = 45°$, when the backward cylinder comes near, the vorticity is peeled away from the cylinder. In addition, in the reverse direction flow, in the vicinity of the rotation angle $\alpha = 0°$, seen in Fig. 7a, the mainstream and the fin are in flowing in opposite directions, and vorticity from the fin tip (yellow—counterclockwise vorticity) occurs. After that, the vorticity is peeled away as the fins move to the vicinity of $\alpha = 45°$ (Fig. 7b). In the flow field around the straight fin, a large effect occurs because the vortex is generated in the vicinity of the cylinder in the forward direction. On the contrary, since the vortex in the opposite direction is far from the cylinder, the impact is small. The positioning of the lift generated by the vortices is estimated by its effects. On the other

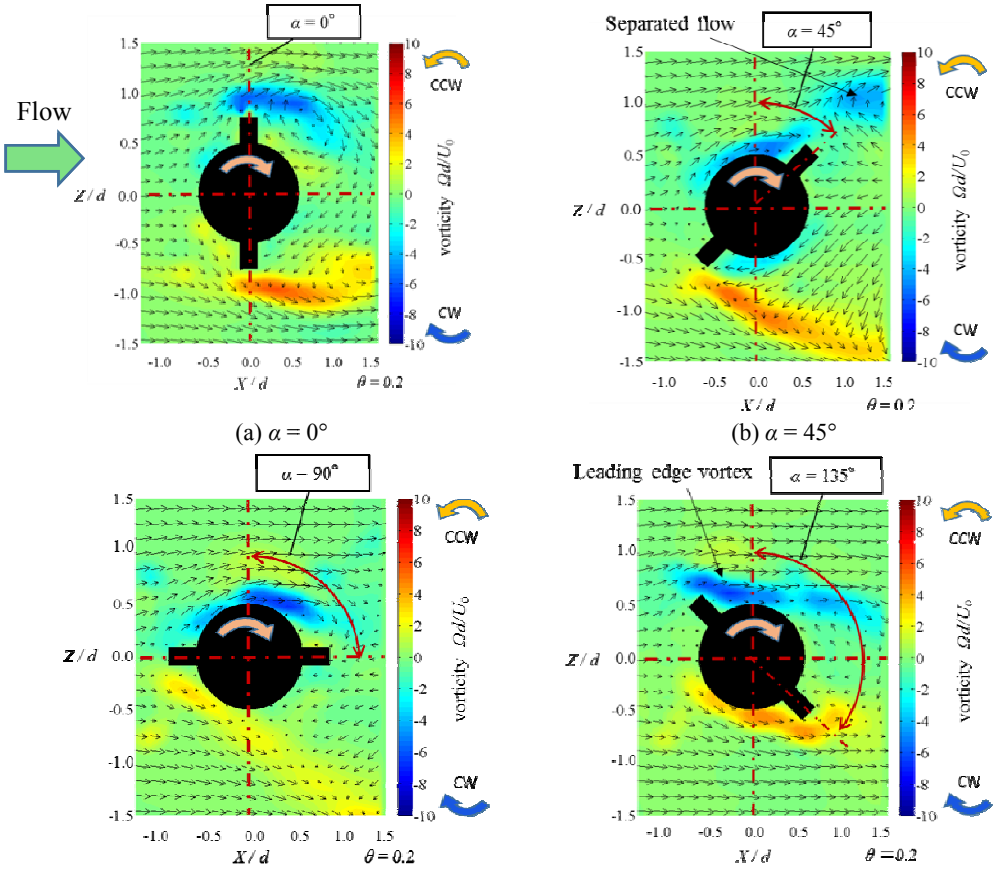

Fig. 7 Flow around rotating cylinder with straight fins. Velocity distribution and vorticity for: (a) $\alpha = 0°$, (b) $\alpha = 45°$, (c) $\alpha = 90°$ and (d) $\alpha = 135°$ ($\theta = 0.2$).

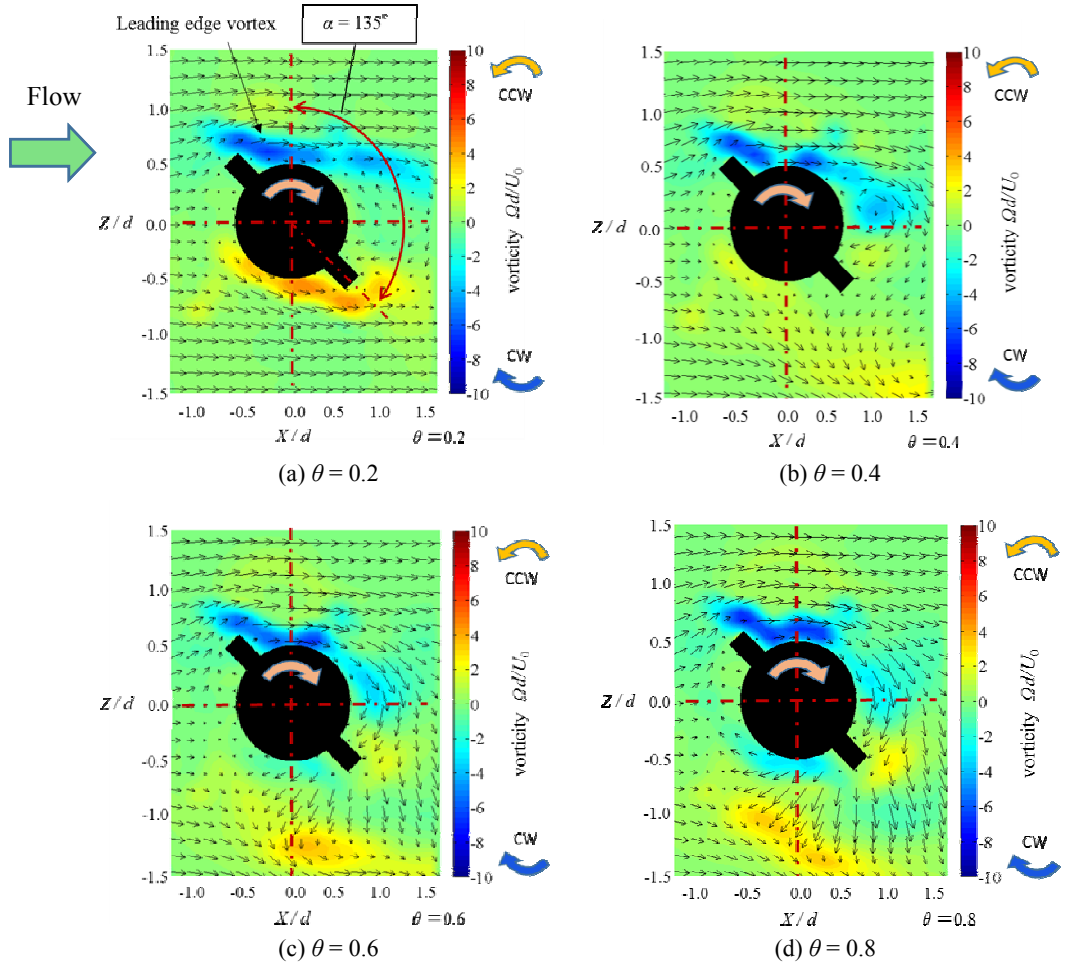

(a) $\theta = 0.2$ (b) $\theta = 0.4$

(c) $\theta = 0.6$ (d) $\theta = 0.8$

Fig. 8 Flow around rotating cylinder with straight fins. Velocity distribution and vorticity, for: (a) θ = 0.2, (b) θ = 0.4, (c) θ = 0.6 and (d) θ = 0.8 (α = 135°).

hand, Fig. 4 shows high life circumferential speed ratio 0.2-0.4. For 0.6-0.8, the increase in lift becomes a plateau. At the low circumferential speed ratio, this system has exceeded the lift of an ideal fluid. This phenomenon is considered the influence of the leading edge vortex that occurs at the backward fin in the vicinity of the rotation angle α = 135°. Thus, it shows the calculation results of the vorticity for the rotation angle α = 135° (Figs. 8a: θ = 0.2, 8b: θ = 0.4, 8c: θ = 0.6 and 8d: θ = 0.8). In studies of conventional airfoils, a series of flow field leading edge vortices are attached to the blade surface, to contribute to the generation of a large lift [7]. Vorticity (blue—clockwise vorticity) is strongly in the forward direction flow of the rotating cylinder. This is means that, in the vicinity of the rotation angle α = 135°, the leading edge vortex is estimated to impact due to the fact that, occurs in the rear fin behind when the mainstream is to pass through the fins. In addition, owing to the occurrence of the leading edge vortex, circulation around the rotor blades increases, which also increases lift.

When photographing a spiral fin, the blind area is widened. This occurs because a shadow is generated by the shape of the fins. Therefore, we attempted to reduce the blind area by individually photographing four synthesized four, as shown in Fig. 9. The cylinder is rotated forward when taking pictures of (area ① of Fig. 9) the upstream upper surface. Subsequently, the fin was in reverse rotation when photographing the upstream lower surface (area ② of Fig. 9). Up to this point, the winding direction of the fin is left. However, in the downstream of the shooting, the fin is in front

of the laser sheet. Therefore it is not possible to shoot. So, we continued taking photographs after changing the direction to the right winding of the fin on the basis of the line that separates the area ③ from the area ① of Fig. 9. Incidentally, we then had a forward rotation and downstream upper surface (area ③ of Fig. 9), and a reverse rotation and downstream lower surface (area ④ of Fig. 9), which we synthesized.

Fig. 10 is the flow field around a rotating cylinder with spiral fins in the mainstream. For spiral fins, the flow field at each rotation angle is similar, we show the results for rotational angle α = 0°, and a circumferential speed ratio θ = 1. With the results in Fig. 10 for the spiral fin, we compared it to Figs. 6a-6d, the straight fin result. We examined the distribution of the main flow direction of the flow rate in the gradient.

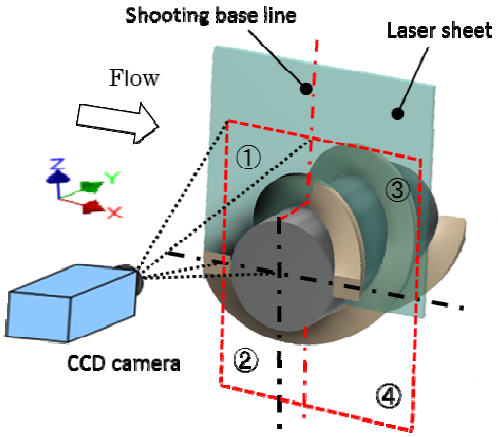

Fig. 9 Method of shooting photography when flow around rotating cylinder with spiral fins.

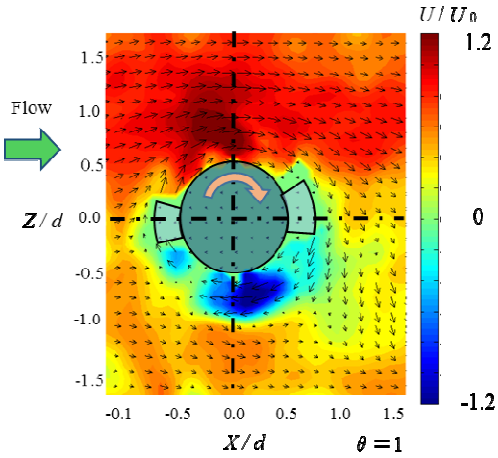

Fig. 10 Flow around rotating cylinder with spiral fins. Velocity distribution (α = 0°).

The straight fins appeared to affect the flow velocity distribution in a far area from the cylinder away from the cylinder. This occurs with a straight fin because the flow to diffuse the normal shape when given the rotation is generated. In comparison, for the spiral fin in the flow affected by the fin, the span direction (Y-axis direction) component is added. Therefore, the normal shape of the diffusion is suppressed, the action of the fins is concentrated in a narrow region near the cylindrical surface, and a large flow velocity difference occurs in the upper and lower streams. In addition, since the straight fins are positioned perpendicular to the main flow, the flow field is changed intermittently by the rotation. Meanwhile, for the spiral fin, the change in the flow field is continuous.

4. Conclusions

In this study, we aimed to elucidate the lift-generating mechanism in the flow field around a winged rotating cylinder. Fluid force measurements of the three types of models were performed. Moreover, the flow field was analyzed with PIV processing. The results are summarized as follows:

For the rotating cylinder winged fins, an increase of lift continues until the circumferential speed ratio θ = 1. Then, it slowly declines. Then, lift is gradually reduced at θ > 1, because the role of the fins begins to decrease gradually.

For the rotating cylinder with fins, the function of the forward flow side of the fin in the case of θ = 1 is small. However, the fin on the reverse flow side, generates a large stagnation area. As a result, it contributes to an increase in the flow rate difference and circulation, which increases the lift. Straight fin lift measurement results exceeded the lift of the ideal fluid at the time the circumferential speed ratio θ = 0.2-0.4. This is the effect of the leading edge vortex that occurs when the mainstream overcomes the rotating cylinder with a straight fin.

The cylinder with spiral fins showed a high lift compared with the cylinder with a straight fin. When

seen from the results of the PIV processing, the intermittent flow field of the straight fin is changed by the rotation angle, and the range of the velocity fluctuation, and reaches a relatively far area from the cylinder.

Meanwhile, the change of the spiral fins around the flow field is continuous. In the area near the cylinder, a large speed difference has been shown to occur. This is the main cause of the high lift of the spiral fin.

References

[1] Nobuhiro, M. 2004. Magnus type wind power generation. Patent 2005-517,614, file June 14, 2004, and issued June 14, 2004.

[2] Michihiko, N. 2015. "Spiral Magnus Windmill." *Japan Wind Energy Association* 39 (113): 14-7.

[3] Shigemitu, S., Jun, I., Nobuhiro, M., Hiromichi, K., and Shinichi, K. 2004. "A Study on the Magnus Effect in a Rotating Cylinder with a Load Structure." In *Proceedings of the 26th Wind Energy Utilization Symposium,* 155-8.

[4] Akiyosi, I., Chisachi, K., Nobuhiro, M., and Tadahiko, N. 2010. "Evaluation of Aerodynamic Properties of Magnus Wind Mill with Spiral Fins." *Transactions of the Japan Society of Mechanical Engineers B* 76 (763): 379-82.

[5] Hiroaki, H., Yusuke, O., and Kazuo, M. 2006. "Relationship between Dynamic Lift and Streamwise Vortices Acting on a Disk Simulating a Hand of Swimmer." *Journal of Japan Society of Fluid Mechanics* 25 (4): 357-66.

[6] Hiroaki, H., Jun, W., and Kazuo, M. 2010. "Effect of 3-Dimensional Airfoil Shape on Unsteady Fluid Forces in Pitching Motion." *Journal of Fluid Science and Technology* 5 (2): 270-80.

[7] Tatjana, Y. H., and Cameron, T. 2010. "The Importance of Leading Edge Vortices under Simplified Flapping Flight Conditions at the Size Scale of Birds." *The Journal of Experimental Biology* 213 (July): 1930-9.